Journal of Alloys and Compounds 504 (2010) 462–467

Contents lists available at ScienceDirect

Journal of Alloys and Compounds

journal homepage: www.elsevier.com/locate/jallcom

Phase transformations of $Fe_{73.5}Cu_1Nb_3Si_{15.5}B_7$ amorphous alloy upon thermal treatment

Aleksandra Gavrilović[a], Dusan M. Minić[b], Lidija D. Rafailović[a,c], Paul Angerer[a], Jaroslaw Wosik[a], Aleksa Maričić[b], Dragica M. Minić[d,*]

[a] CEST Centre of Electrochemical Surface Technology, A-2700 Wiener Neustadt, Austria
[b] Technical Faculty of Čačak, University of Kragujevac, 32000 Čačak, Serbia
[c] Physics of Nanostructured Materials, Faculty of Physics, University of Vienna, A-1090 Vienna, Austria
[d] Faculty of Physical Chemistry, University of Belgrade, 11001 Belgrade, Serbia

ARTICLE INFO

Article history:
Received 6 November 2009
Received in revised form 21 May 2010
Accepted 29 May 2010
Available online 11 June 2010

Keywords:
Amorphous materials
Metallic glasses
Metals and alloys
Thermal analysis
Phase transition

ABSTRACT

The structural transformations of $Fe_{73.5}Cu_1Nb_3Si_{15.5}B_7$ amorphous alloy under non-isothermal as well as isothermal conditions were studied. Differential scanning calorimetry (DSC) showed that slow heating rates induce a series of stepwise structural transformations consisting of endothermic peaks and more pronounced exothermic peaks in the broad temperature range from 350 to 970 K. Over this range the system changed from an as-deposited amorphous alloy of higher excess free energy to an annealed sample exhibiting lower excess of free energy. X-ray diffraction (XRD) analysis found that primary crystallization started with formation of a face-centred Fe_3Si phase in an amorphous matrix. At higher temperatures (between 780 and 920 K) we detected, in addition to the Fe_3Si phase, which reached an almost constant value of 85 wt%, three new phases, $FeCu_4$, $Fe_{16}Nb_6Si_7$ and Fe_2B. Further annealing above 923 K led to, with Si initially migrating from the Fe–Si phase to the Nb-rich grain boundaries, formation of two new phases, Fe_5Si_3 and Nb_5Si_3. The Fe content in the cubic Fe–Si phase was estimated by means of a change in lattice parameter. Below 923 K the size of crystallites for the major Fe_3Si phase was less than 10 nm. It was shown that further heating induced rapid crystallite growth, reaching a size greater than 500 nm at 1123 K.

1. Introduction

The soft magnetic amorphous materials (metallic glasses) are considered the future of magnetic materials in power electronics on account of their marvellous magnetic properties. The majority of metallic glasses are materials which are kinetically and thermodynamically metastable. The structure of some of these materials may change spontaneously with time, but most of them are stable at room temperature and can be transformed directly to polycrystalline materials at higher temperatures [1,2]. The polycrystalline soft magnetic materials with grain size less than 100 nm, called nanocrystalline, possess superior soft magnetic properties, for example, "Finemet®" and "Nanoperm®" alloys and their modifications [3–9]. These materials generally contain two structural components: one consisting of periodically positioned atoms inside the crystallites and the other with all atoms located in the interfacial regions, having strongly distorted structures [10]. Owing to the small grain size, the local magneto-crystalline anisotropy is averaged out by exchange interactions leading to low or vanishing saturation magnetostriction [11].

The nanocrystalline soft magnetic materials can be obtained by crystallization of amorphous alloys when the nucleation rate is high and crystal growth rate low. In addition to the control of heat treatment conditions such as heating rate, specific annealing temperature and time, the addition of small quantities of elements such as Cu and Nb, favours the formation of a nanocrystalline structure in these materials [1,12].

The Fe-based nanocrystalline soft magnetic alloys such as "Finemet" ($Fe_{73.5}Cu_1Nb_3Si_{13.5}B_9$) contain small amounts of Cu which is immiscible with Fe and Nb [5,13]. The Cu, despite its low content, affects the crystallization process and is responsible for the formation of nanostructured materials. Due to its very limited solubility in Fe, Cu forms small clusters which serve as sites for heterogeneous nucleation of α-Fe–Si crystallites, increasing their number in amorphous matrix. Furthermore, Nb, which is rejected from the crystal phase into the amorphous matrix, decreases the crystal growth because of its relatively low diffusivity [14].

The extensive application of nanostructural metallic alloys of this type is primarily due to their unique soft magnetic properties, which make them suitable for use in sensors. It was shown

* Corresponding author. Tel.: +381 11 3336 689; fax: +381 11 2187 133.
E-mail addresses: dminic@ffh.bg.ac.rs, drminic@gmail.com (D.M. Minić).

0925-8388/$ – see front matter © 2010 Elsevier B.V. All rights reserved.
doi:10.1016/j.jallcom.2010.05.145

that two main phases exist in Fe–Cu–Nb–Si–B alloys with optimum magnetic properties, one of them being the nanocrystalline ferromagnetic α-Fe–Si solid phase (volume fraction 60–65%) with an average grain size typically of 10–15 nm embedded in an amorphous ferromagnetic matrix [15].

Since soft magnetic materials can possess very attractive physical properties, great efforts have been made to predict and control the crystallization processes of metallic glasses [16]. The formed microstructures are very sensitive to annealing temperature as well as the thermal history of the materials; therefore a study of microstructure evolution of the nano-magnetic materials can provide good guidance for tailoring desired properties [17,18].

The objective of this work was to conduct a detailed study of the crystallization process of amorphous $Fe_{73.5}Cu_1Nb_3Si_{15.5}B_7$ alloy in the temperature range 273–1123 K. Our main interest was the behaviour of the alloy at high temperatures. Therefore, special attention was paid to samples of alloy annealed at temperatures above 873 K.

2. Experimental procedures

By means of the standard procedure of rapid quenching of the melt on a rotating disc (melt-spinning method), amorphous ribbon samples with a stoichiometric composition $Fe_{73.5}Cu_1Nb_3Si_{15.5}B_7$ (Vitroperm®) and with dimensions of 2.5 cm width and 35 μm thicknesses were prepared. Composition analysis by EDX confirmed that the expected elements were present in the amorphous alloy. The amorphous ribbon samples were sealed in quartz tubes under technical vacuum and isothermally annealed for 1 h at temperatures of 693, 753, 773, 813, 873, 923, 973, 1023, 1073, and 1123 K, respectively.

Differential thermal calorimetry of the samples was conducted using a DSC-204 C device (Netzsch, Germany) in the temperature range 298–973 K under an Ar atmosphere at a constant heating rate of 4 K min^{-1}. A uniform temperature distribution was insured by using sample of reduced mass (approximately 5 mg). A slow heating rate of 4 K min^{-1} increased the sensitivity for detection of smaller exothermic and endothermic changes in DSC. Two heating runs were employed to obtain a baseline; the first heating run was with an as-prepared sample and the second heating run was conducted after cooling the sample to ambient temperature [19].

XRD experiments were performed on an X-Pert powder diffractometer (PANalytical, Netherlands) using CuKα radiation in Bragg–Brentano geometry at 40 kV and 30 mA. The measurements were conducted in a step scan mode in 0.05° (2θ) intervals with a measuring time of 30 s/step. This diffractometer is equipped with a secondary graphite monochromator, automatic divergence slits, and a scintillation counter.

The TOPAS V3 general profile and structure analysis software for powder diffraction data was used for the Rietveld refinement procedure [20].

Microstructural examination was performed by scanning electron microscope (SEM). An XL 30 ESEM-FEG (environmental scanning microscope with field emission gun, manufactured by FEI, Netherlands) device equipped with an energy dispersive X-ray spectrometer from EDAX was used. The samples were inspected using 5, 10 and 20 kV acceleration voltages at magnifications of 20,000× and 10,000×, respectively.

3. Results and discussion

The thermal behaviour of the $Fe_{73.5}Cu_1Nb_3Si_{15.5}B_7$ amorphous alloy is depicted in the DSC curves (Fig. 1). As the amorphous sample undergoes structural transformations during heating, a broad exothermic maximum in the range 350–550 K is attributed to the structural relaxation processes in as-prepared amorphous alloy. This process is followed by the Curie temperature and the glass transition temperature [21,22]. The process of crystallization involves three well-defined broad asymmetric exothermic peaks (T_{k1}, T_{k2} and T_{k3}) indicating a stepwise process of the structural transformation of the alloy in the broad temperature range from 750 to 1000 K. During these structure transformations the system moves from as-deposited amorphous alloy of higher excess free energy to the annealed sample exhibiting a lower excess of free energy. The absence of peaks in repeated run on the same alloy after cooling has shown that mentioned process really corresponds to crystallization (Fig. 1). The corresponding enthalpy releases of $\Delta H_1 = -67.3\,J\,g^{-1}$ in the temperature range 760–835 K and $\Delta H_2 = -3.4\,J\,g^{-1}$ in the temperature range 875–890 K give a measure of the thermal stability of the sample with respect to structural transformations involving nucleation and growth of crystals in different temperature ranges.

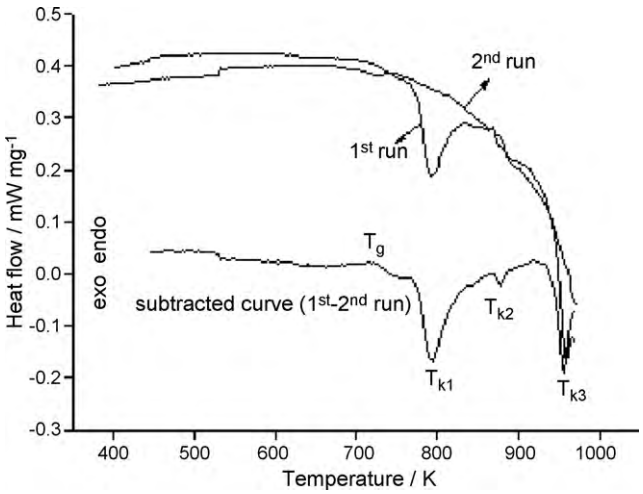

Fig. 1. DSC of as-prepared alloy at heating rate 4 K min^{-1}.

After the DSC analysis involving heating to 973 K, the sample was cooled down to room temperature, and an XRD analysis was performed (Fig. 2). The slow heating rate (4 K min^{-1}) during the DSC analysis caused the structural transformations in the alloy, resulting in the formation of four crystalline phases: Fe_3Si (81.1 ± 2.4 wt%), $FeCu_4$ (1.4 ± 0.3 wt%), Fe_2B (7.9 ± 2.0 wt%) and $Fe_{16}Nb_6Si_7$ (9.6 ± 1.7 wt%). The application of a slow heating rate was suitable for the generation of a large number of crystallization seeds, which resulted in small final crystallites sizes: Fe_3Si (12.1 ± 0.6 nm), $FeCu_4$ (24.6 ± 9.0 nm), Fe_2B (17.1 ± 2.8 nm) and $Fe_{16}Nb_6Si_7$ (2.2 ± 0.2 nm).

The microstructural development was further investigated on isothermally annealed and then quenched samples. Quenching of the samples, which were previously sealed in quartz tubes under technical vacuum and isothermally annealed for 1 h at selected temperatures (chosen in accordance with the DSC analysis) was performed in water at room temperature.

Fig. 3 shows the XRD patterns of an as-prepared alloy sample as well as samples of the material subjected to annealing, during 1 h,

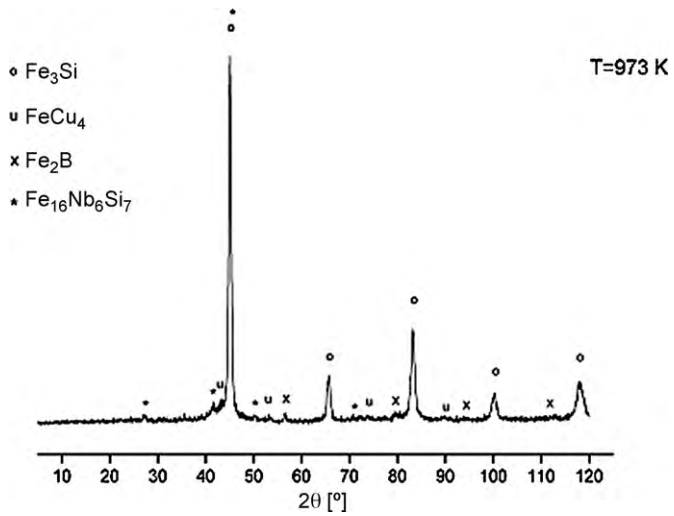

Fig. 2. X-ray diffractogram of the sample heated up to 973 K under an argon atmosphere during DSC analysis and then left cool slowly to room temperature.

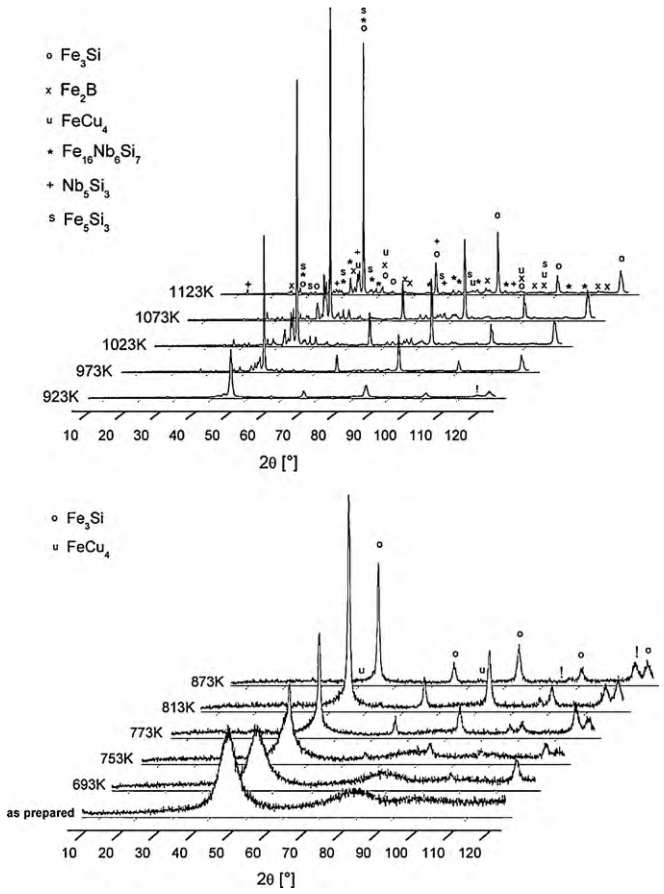

Fig. 3. XRD patterns of $Fe_{73.5}Cu_1Nb_3Si_{15.5}B_7$ alloy samples as-prepared as well as heated during 1 h at different temperatures as indicated.

at different temperatures (693, 753, 773, 813, 873, 923, 973, 1023, 1073, and 1123 K).

XRD as well as SEM investigation of the as-prepared $Fe_{73.5}Cu_1Nb_3Si_{15.5}B_7$ alloy confirmed the absence of long range ordering. The first crystallization process during heating to 693 K was detected by the appearance of two very small diffraction peaks at 97.159° and 115.042° 2θ, as shown in Fig. 3. Unfortunately the majority of ICDD-PDF powder diffraction data do not cover the 2θ angle range of the unidentified reflections noted above. Therefore a complete and accurate identification of this phase was not possible. However, the diffraction pattern corresponds well to a phase with cubic symmetry (face-centred structure, FCC) [23]. This unidentified phase remained present until 923 K. The XRD analysis of the sample annealed at 753 K displayed besides a broad hump in the 2θ range 40–50° (corresponding to the amorphous fraction of the material) also the major crystalline α-Fe–Si phase (FCC or DO_3 crystal structure). The best match to the Fe–Si diffraction pattern is that of a pattern for α-Fe_3Si (ICDD-PDF 03-065-0146). This structure could result from the good solubility of Si in α-Fe in the early stages of crystallization. Furthermore, a significant fraction of the Fe atoms rejected from the DO_3 nanocrystals formed statistically disordered interfacial grain boundaries in the later stages of crystallization [24].

This structural composition remained unchanged up to 873 K, when formation of the crystalline phase $FeCu_4$ (ICDD-PDF 03-065-7002) started. At this annealing temperature the copper-iron phase was not very abundant. At 923 K, slow dissolution of B and Nb atoms into the Fe matrix led to the formation of two new phases: $Fe_{16}Nb_6Si_7$ (ICDD-PDF 00-053-0459) and Fe_2B (ICDD-PDF 00-036-1332).

Table 1
Crystal symmetry, space group (Hermann–Mauguin symbol), and lattice parameters for all observed phases according to the ICDD-PDF database.

Phase	Space group	Crystal system	Lattice parameters [Å]	
			a	*c*
Fe_3Si	Fm-3m	Cubic	5.670	–
$FeCu_4$	Fm-3m	Cubic	3.618	–
$Fe_{16}Nb_6Si_7$	Fm-3m	Cubic	11.338	–
Fe_2B	I4/mcm	Tetragonal	5.110	4.249
Nb_5Si_3	I4/mcm	Tetragonal	10.018	5.072
Fe_5Si_3	P63/mcm	Hexagonal	6.755	4.717

As it is shown in Fig. 3, further structural transformations did not occur between 973 and 1123 K. Annealing at 973 K gave rise to two phases in trace contents: Fe_5Si_3 (ICDD-PDF 03-065-3593) and Nb_5Si_3 (ICDD-PDF 03-065-2785). These two phases were not noticed in the sample after DSC analysis. It could be speculated that the formation of these phases requires a prolonged period of heating. The unit cell parameters for each crystal system as well as the corresponding Hermann–Mauguin space group symbol are given in Table 1.

As stated in the literature, the crystallization in Fe-based amorphous alloys takes place more easily near the surface than within the bulk [25]. The process of crystallization initiates at the surface during heat treatment and then propagates into the bulk.

The quantitative phase analysis was performed together with crystallite size and lattice constant determination using the program TOPAS V3 (Bruker AXS GmbH, Germany) by means of Rietveld refinement of the XRD data. This program uses the "fundamental parameter approach" which enables a full convolution based synthesis of line profiles [20].

The mean shape of the crystallites must be known in order to derive and apply a correction to the column height of each hkl. Since the crystallite size ε cannot be measured directly, TOPAS V3 uses the integrated breadth based L_{vol} calculation (according to Eq. (1)) assuming intermediate crystallite size broadening modelled by a Voigt function [20]:

$$w_i = \lambda/(L_{vol}\cos\theta) \tag{1}$$

where w_i are integral breadths defined as:

$$w_i = \frac{w}{k}; \tag{2}$$

λ is the wavelength of the used Cu radiation, θ the Bragg angle and L_{vol} is volume weighted mean column height defined as:

$$L_{vol} = \varepsilon k. \tag{3}$$

In Eq. (2), w is the FWHM (full width at half maximum) of the instrument corrected line profile and k is the Scherrer constant.

Fig. 4 shows a change in relative phase contributions [wt%] during the thermal treatment as determined by the Rietveld refinement procedure. With an increase in temperature, the relative contribution of the Fe_3Si phase, which is observed primarily at 773 K, decreases very slowly reaching an almost constant value of 85.0 ± 0.6 wt% for annealing temperatures above 923 K. The relative amounts of the other phases were low: $FeCu_4$ (1.7 ± 0.4 wt% with maximum 6.6 ± 0.6 wt%), Fe_2B (1.4 ± 0.6 wt% with maximum 4.9 ± 1.0 wt%), $Fe_{16}Nb_6Si_7$ (4.7 ± 0.5 wt% with maximum 11.5 ± 0.6 wt%), Nb_5Si_3 (0.8 ± 0.2 wt% with maximum 2.0 ± 0.2 wt%) and Fe_5Si_3 (0.5 ± 0.2 wt% with maximum 1.6 ± 0.2 wt%). Complete information for all relative weight fraction contributions presented in this paper was shown in Table 2.

The crystallization process for the $Fe_{73.5}Cu_1Nb_3Si_{15.5}B_7$ alloy started with formation of DO_3 nanosized crystallites whose further growth is temperature dependent as shown in Table 3. The crystallite size of the major Fe_3Si phase remained almost constant,

Table 2
Relative weight fractions (wt%) corresponding to each phase and for different heating conditions presented in this paper.

Temperature [K]	Annealing time [h]	Fe_3Si	$FeCu_4$	$Fe_{16}Nb_6Si_7$	Fe_2B	Nb_5Si_3	Fe_5Si_3
		Relative weight fraction [wt%]					
773	1	100	–	–	–	–	–
813	1	100	–	–	–	–	–
873	1	96.4 ± 1.3	3.6 ± 1.3	–	–	–	–
923	1	80.6 ± 1.1	3.0 ± 0.3	11.5 ± 0.6	4.9 ± 1.	–	–
973	1	84.2 ± 0.9	6.6 ± 0.6	4.7 ± 0.5	2.1 ± 0.6	0.8 ± 0.2	1.6 ± 0.2
1023	1	86.9 ± 0.7	2.3 ± 0.4	6.5 ± 0.4	2.6 ± 0.4	1.1 ± 0.2	0.6 ± 0.2
1073	1	86.9 ± 0.8	1.7 ± 0.4	7.5 ± 0.3	1.4 ± 0.6	2.0 ± 0.2	0.5 ± 0.2
1123	1	85.0 ± 0.6	2.8 ± 0.3	7.6 ± 0.3	2.6 ± 0.4	1.5 ± 0.2	0.5 ± 0.1
1123[a]	24	87.1 ± 0.4	3.3 ± 0.3	5.4 ± 0.3	2.7 ± 0.4	0.9 ± 0.2	0.6 ± 0.1
973[b]	–	81.1 ± 2.4	1.4 ± 0.3	9.6 ± 1.7	7.9 ± 2.0	–	–

[a] The sample was analysed after annealing at 1123 during 24 h.
[b] The sample was analysed by DSC technique in the temperature range of 298–973 K in an argon atmosphere with a constant heating rate of 4 K min^{-1}.

Table 3
Crystallite sizes for the observed phases upon heating at different temperatures.

Temperature [K]	Annealing time [h]	Fe_3Si	$FeCu_4$	$Fe_{16}Nb_6Si_7$	Fe_2B	Nb_5Si_3	Fe_5Si_3
		Crystallite size [nm]					
773	1	9.0 ± 1.3	–	–	–	–	–
813	1	9.6 ± 1.2	–	–	–	–	–
873	1	9.4 ± 1.2	4.0 ± 1.5	–	–	–	–
923	1	18.5 ± 1.5	7.7 ± 1.9	5.3 ± 1.5	4.5 ± 1.6	–	–
973	1	75.8 ± 2.6	5.9 ± 3.8	20.3 ± 2.1	22.7 ± 1.5	31.4 ± 1.8	11.6 ± 2.7
1023	1	244.2 ± 2.9	22.6 ± 1.6	25.3 ± 2.9	27.5 ± 2.8	44.8 ± 2.2	54.4 ± 2.1
1073	1	463.9 ± 2.9	36.8 ± 2.4	49.7 ± 5.6	44.8 ± 5.2	46.8 ± 2.2	57.0 ± 2.5
1123	1	523.8 ± 3.9	40.4 ± 3.0	64.8 ± 7.9	54.4 ± 5.3	44.8 ± 7.7	115.5 ± 6.6
1123[a]	24	600.0 ± 5.1	69.4 ± 4.5	93.3 ± 2.0	61.0 ± 4.5	59.6 ± 3.4	115.9 ± 7.9
973[b]	–	12.1 ± 0.6	24.6 ± 9.0	2.2 ± 0.2	17.1 ± 2.8	–	–

[a] The sample was analysed after annealing at 1123 during 24 h.
[b] The sample was analysed by DSC technique in the temperature range of 298–973 K in an argon atmosphere with a constant heating rate of 4 K min^{-1}.

about 9 nm, after annealing for 1 h at temperatures between 773 and 873 K. In this temperature range, Nb in the amorphous grain boundaries significantly restricts the growth of the Fe_3Si crystallites. Furthermore, the crystallite growth increases rapidly above 923 K. This coincides well with formation of the $Fe_{16}Nb_6Si_7$ phase.

The sample annealed at 1123 K for 24 h (Fig. 5) displayed besides the Fe–Si phase only minor contributions of other phases (ranging from 0.5 to 7.6 wt% for each phase).

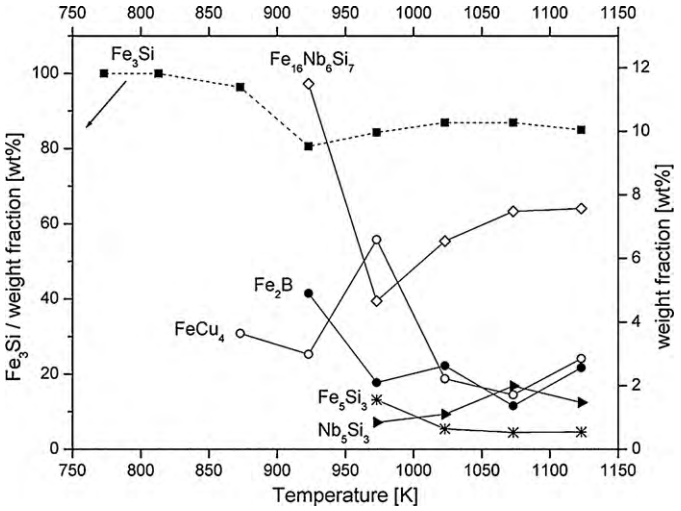

Fig. 4. Relative weight fractions of the observed crystalline phases as determined by the Rietveld refinement method. The left ordinate corresponds to the relative phase contribution of the Fe_3Si during thermal treatment; the right ordinate is related to the relative phase contributions of each of the other phases.

The resulting diffraction pattern (Fig. 5) reveals very sharp and intense peaks belonging to the major, well crystallized, Fe_3Si phase. This indicates, as the Rietveld refinement confirmed, that further grain growth occured during heating treatment. The final value of the crystallite size (24 h dwell) for the major phase reached 600.0 ± 5.1 nm with 87.1 ± 0.4 wt% relative phase contribution.

Evolution of the lattice constant *a* for the Fe–Si phase (DO_3 structure) as determined by the Rietveld procedure is displayed in Fig. 6. According to the relation derived in our former work [26] we calculated the Fe content in the Fe–Si phase, (right ordinate scale in Fig. 6). It is most likely that during crystallization Si initially diffuses

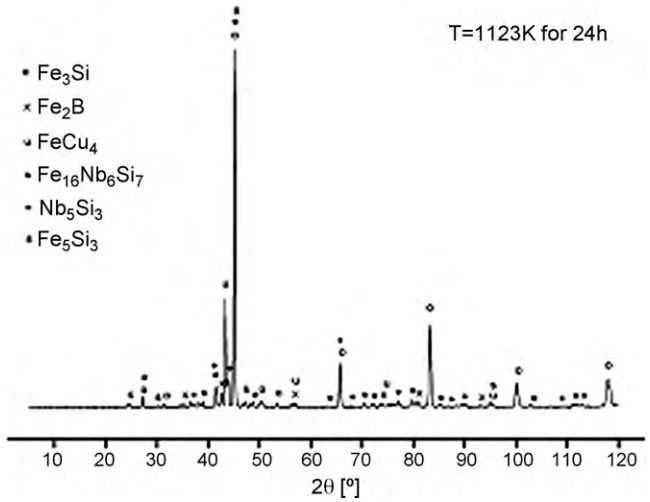

Fig. 5. XRD pattern of the $Fe_{73.5}Cu_1Nb_3Si_{15.5}B_7$ alloy sample heated for 24 h at 1123 K.

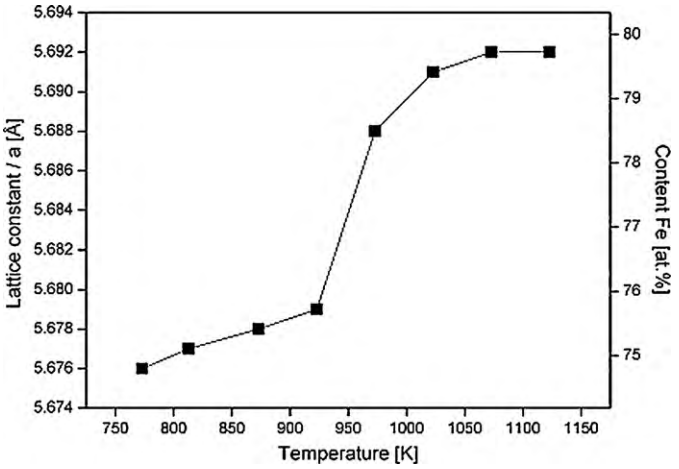

Fig. 6. Lattice constant *a* of the cubic Fe–Si phase and corresponding content of Fe, plotted as a function of the heating temperature.

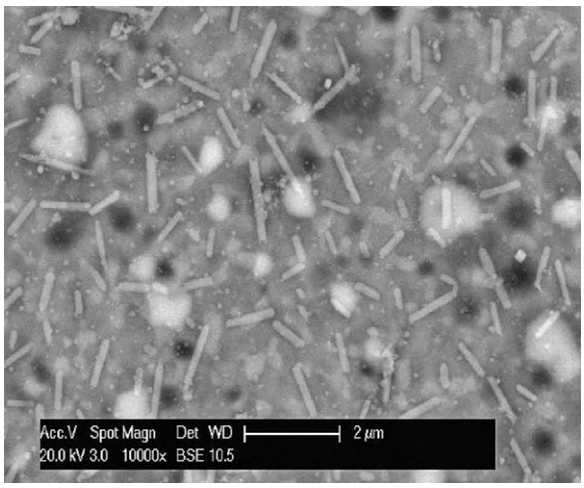

Fig. 7. SEM micrograph of surface, after heat treatment at 1123 K for 24 h.

from the crystalline Fe–Si phase to Nb-rich grain boundaries and with rise the temperature (above 923 K) forms two new phases, Fe_5Si_3 and Nb_5Si_3. As a consequence, the Fe content in the Fe–Si phase increases from 75% to 80% with an increase in temperature, and the cell parameter increases from 5.676 to 5.692 Å. It should be noted, that minor changes of the lattice constant could also be caused by minor incorporation of Nb and B into the Fe–Si phase, but this effect should be significantly smaller.

SEM micrograph of the sample surface after heat treatment for 24 h at 1123 K (cf. Fig. 7) shows the presence of crystal grains of different shapes and shadings corresponding to the different phases found by X-ray analysis. The corresponding EDX analysis showed significant variations in composition. The black rifts in the sample surface are enriched with Si, Nb and Fe. The white, large and almost spherical particles contain Cu exclusively. EDX analysis of the dark-grey, basic area shows mainly Si and Fe content while in the needle-like particles Nb is predominant.

The addition of small amounts of Nb to the Fe–Cu–Si–B system leads to generation of atomic pairs (Nb–Fe, Nb–B), leading to the formation of a highly dense amorphous random packed structure, which results in high microhardness. Fe–Cu–Nb–Si–B metallic glasses are well known as very hard (Vickers hardness higher than 800 HV), but brittle materials [27].

Annealing of the amorphous material at 753 K leads to the beginning of crystallization. As a result of the atomic rearrangement a partially crystalline material was formed with a large number of dislocations, accompanied by a reduction in ductility.

The dislocation density decreases with the increase of annealing temperature, as it can be seen from Table 4. This is strongly related to the crystallite size growth and the total crystalline to amorphous phase volume ratio, leading to the decrease of the mechanical hardness and the increase of ductility of alloy.

4. Conclusions

During the structural transformations of the $Fe_{73.5}Cu_1Nb_3Si_{15.5}B_7$ alloy, the system changed from an as-deposited amorphous alloy to an annealed material exhibiting lower excess of free energy. The primary crystallization started by formation of Fe_3Si phase (face-centred structure) in an amorphous matrix. At higher temperatures (above 920 K) the content of Fe_3Si phase is almost constant, accounting for 85 wt% of the crystalline phases. Additionally, new phases $FeCu_4$, $Fe_{16}Nb_6Si_7$ and Fe_2B were detected. With further annealing above 923 K, Si diffuses from the Fe–Si phase to the Nb-rich grain boundaries, and has been involved in formation of the new minor phases Fe_5Si_3 and Nb_5Si_3. The sample of alloy annealed for 1 h under vacuum, at 973 K, and then quenched at room temperature, was compared with the sample of alloy annealed by heating up to 973 K under Ar at a constant heating rate of 4 K min^{-1} during DSC analysis. It was found that in both cases the dominant phase was Fe_3Si (more than 80 wt% content). However, the crystallite size of this phase for the annealed sample was significantly larger (75.8 ± 2.6 nm) than for the DSC sample (12.1 ± 0.6 nm). It is most likely that the duration of the thermal treatment as well as the annealing atmosphere affected the final crystallite size. The slow heating during DSC analysis induced a large number of crystallization seeds, which resulted in a smaller final crystallite size. The size

Table 4
Dislocation density for the $Fe_{73.5}Cu_1Nb_3Si_{15.5}B_7$ alloy after heat treatment (experimental conditions as given in Table 3).

Temperature [K]	Fe_3Si	$FeCu_4$	$Fe_{16}Nb_6Si_7$	Fe_2B	Nb_5Si_3	Fe_5Si_3
	Dislocation density [m^{-2}]					
773	3.70×10^{16}	–	–	–	–	–
813	3.26×10^{16}	–	–	–	–	–
873	3.40×10^{16}	1.88×10^{17}	–	–	–	–
923	8.77×10^{15}	5.06×10^{16}	1.07×10^{17}	1.48×10^{17}	–	–
973	5.22×10^{14}	8.62×10^{16}	7.28×10^{15}	5.82×10^{15}	3.04×10^{15}	2.23×10^{16}
1023	5.03×10^{13}	5.87×10^{15}	4.69×10^{15}	3.97×10^{15}	1.49×10^{15}	1.01×10^{15}
1073	1.39×10^{13}	2.22×10^{15}	1.21×10^{15}	1.49×10^{15}	1.37×10^{15}	9.23×10^{14}
1123	1.09×10^{13}	1.84×10^{15}	7.14×10^{14}	1.01×10^{15}	1.49×10^{15}	2.25×10^{14}
1123[a]	8.33×10^{12}	6.23×10^{14}	3.45×10^{14}	8.06×10^{14}	8.45×10^{14}	2.23×10^{14}
973[b]	–	2.05×10^{16}	4.96×10^{15}	1.03×10^{16}	–	–

[a] The sample was analysed after annealing at 1123 during 24 h.
[b] The sample was analysed by DSC technique in the temperature range of 298–973 K in an argon atmosphere with a constant heating rate of 4 K min^{-1}.

of the Fe_3Si crystallites for the quenched samples (initially being around 10 nm) increased with the increase of temperature and the duration of thermal treatment, reaching more than 500 nm when annealed for 1 h at 1123 K. The samples annealed in technical vacuum underwent surface crystallization, with the final grain size increased by expansion into the bulk.

Acknowledgements

The investigation was partially supported by the Ministry of Science and Environmental Protection of Serbia, the Project 142025. The work at CEST was supported within the COMET program by the Austrian Research Promotion Agency (Österreichische Forschungsförderungsgesellschaft, FFG) and the government of Lower Austria.

References

[1] T. Kulik, J. Non-Cryst. Solids 287 (2001) 145–161.
[2] I. Škorvánek, J. Marcin, J. Turcanová, J. Kovác, P. Švec, J. Alloys Compd. (2010), doi:10.1016/j.jallcom.2010.04.033.
[3] H.F. Li, D.E. Laughlin, R.V. Ramanujan, Philos. Mag. 86 (2006) 1355–1372.
[4] M.E. McHenry, M.A. Willard, D.E. Laughlin, Prog. Mater. Sci. 44 (1999) 291.
[5] T. Gloriant, S. Suriñach, M.D. Baró, J. Non-Cryst. Solids 333 (2004) 320–326.
[6] R. Brzozowski, M. Wasiak, H. Piekarski, P. Sovak, P. Uznański, M.E. Moneta, J. Alloys Compd. 470 (2009) 5–11.
[7] A. Kolano-Burian, R. Kolano, L.K. Varga, J. Alloys Compd. 483 (2009) 560–562.
[8] H.A. Shivaee, H.R.M. Hosseini, E.M. Lotfabad, S. Roostaie, J. Alloys Compd. 491 (2010) 487–494.
[9] A. Puszkarz, M. Wasiak, A. Różański, P. Sovak, M. Moneta, J. Alloys Compd. 491 (2010) 495–498.
[10] Ch. Polak, M. Knobel, R. Grössinger, R. Sato Turtelli, J. Magn. Magn. Mater. 134 (1994) 1–12.
[11] G. Herzer, J. Magn. Magn. Mater. 133 (1994) 248–250.
[12] Y.R. Zhang, R.V. Ramanujan, Intermetallics 14 (2006) 710–714.
[13] Y. Yoshiyawa, S. Oguma, K. Yamauchi, J. Appl. Phys. 64 (1988) 6044.
[14] H. Hermann, A. Heinemann, N. Mattern, A. Weidenmann, Europhys. Lett. 51 (2000) 127.
[15] T. Liu, Z.X. Xu, R.Z. Ma, J. Magn. Magn. Mater. 152 (1996) 365–369.
[16] D.R. dos Santos, D.S. dos Santos, Mater. Res. 4 (2001) 47–51.
[17] M.L. Sui, K.Y. He, L.Y. Xiong, Y. Liu, J. Zhu, Mater. Sci. Eng. A181/A182 (1994) 1405–1409.
[18] S.W. Du, R.V. Ramanujan, J. Non-Cryst. Solids 351 (2005) 3105–3113.
[19] L.D. Rafailović, W. Artner, G.E. Nauer, D.M. Minić, Thermochim. Acta 496 (2009) 110.
[20] Bruker AXS, TOPAS V3. General profile and structure analysis software for powder diffraction data, Karlsruhe, 2005.
[21] F.F. Marzo, A.R. Pierna, A. Altube, J. Non-Cryst. Solids 287 (2001) 349–354.
[22] C. Miguel, S. Kaloshkin, J. Gonzalez, A. Zhukov, J. Non-Cryst. Solids 329 (2003) 63–66.
[23] D.M. Minić, A. Gavrilović, P. Angerer, D.G. Minić, A. Maričić, J. Alloys Compd. 482 (2009) 502–507.
[24] Y. Swilem, Physica B 371 (2006) 182–186.
[25] A.K. Panda, M. Manimaran, A. Mitra, S. Basu, Appl. Surf. Sci. 235 (2004) 475–486.
[26] D.M. Minić, A. Gavrilović, P. Angerer, D.G. Minić, A. Maričić, J. Alloys Compd. 476 (2009) 705–709.
[27] W. Martienssen, H. Warlimont, Springer Handbook of Condensed Matter and Materials Data, first ed., Springer, Berlin, Heidelberg, 2005.